Supporting Information

"Cu_3-Cluster-Doped Monolayer Mo_2CO_2 (MXene) as an Electron Reservoir for Catalyzing a CO Oxidation Reaction"

Cheng Cheng,[†] Xilin Zhang,[†] Zongxian Yang,*[,†,‡] and Zhen Zhou[§]

[†]College of Physics and Materials Science and [‡]National Demonstration Center for Experimental Physics Education, Henan Normal University, Xinxiang, Henan 453007, China

[§]School of Materials Science and Engineering, National Institute for Advanced Materials, Institute of New Energy Material Chemistry, Collaborative Innovation Center of Chemical Science and Engineering (Tianjin), Nankai University, Tianjin 300350, China

E-mail: yzx@henannu.edu.cn (Z.Y.).

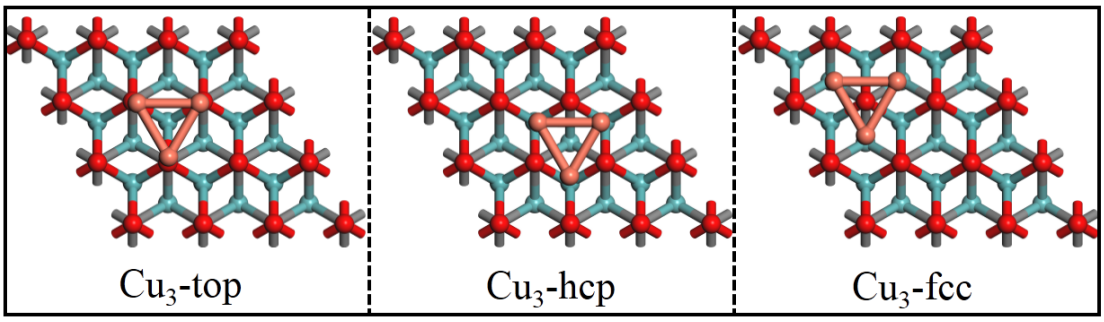

Figure S1. Three deposited sites of Cu_3 cluster on the pristine Mo_2CO_2 monolayer.

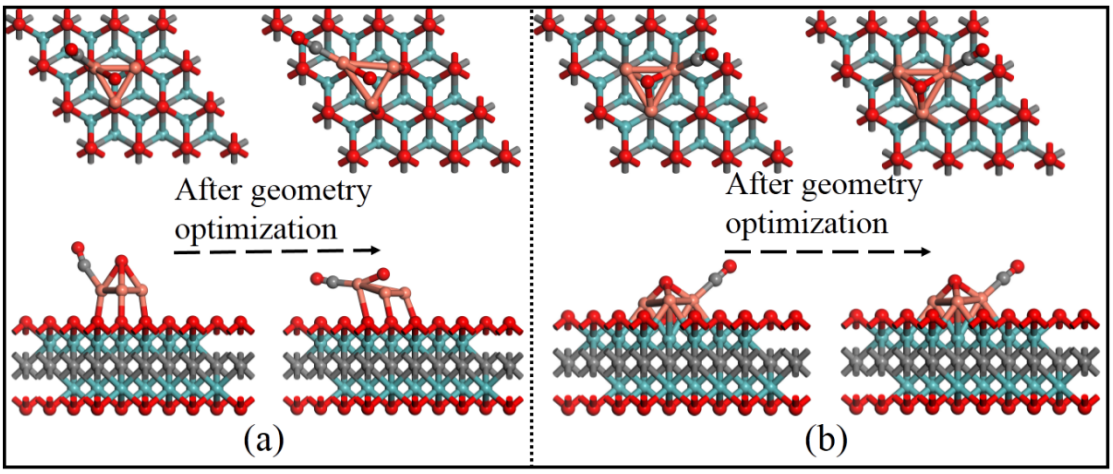

Figure S2. The co-adsorption of O and CO atoms on (a) Cu_3/p-Mo_2CO_2 and (b) Cu_3/d-Mo_2CO_2 configurations, before and after geometry optimization.

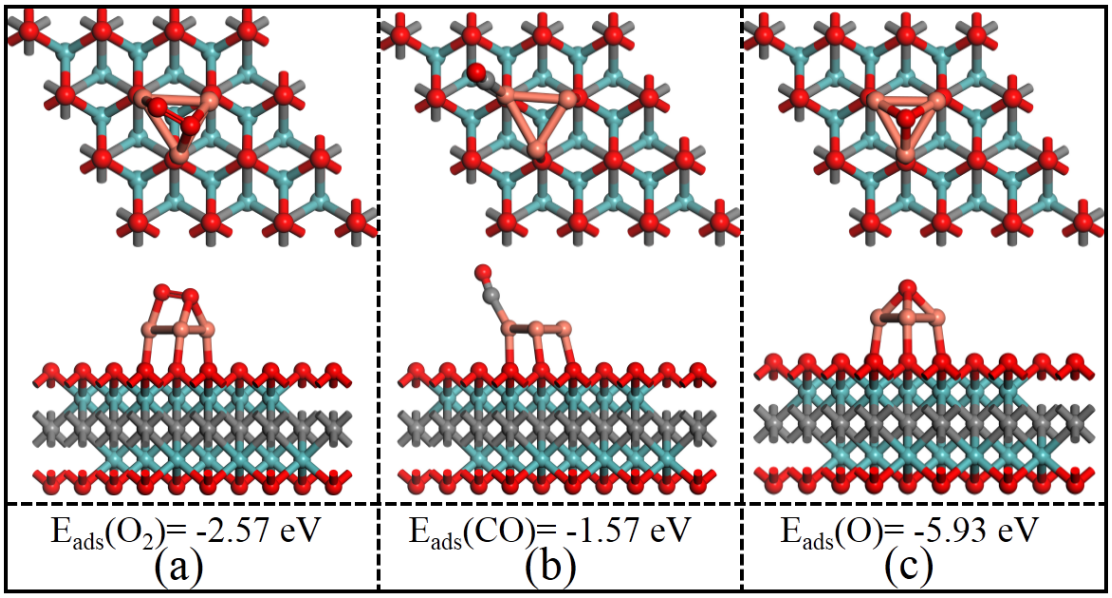

Figure S3. Top and side views of the adsorption configurations and adsorption energies of (a) O_2, (b) CO, and (c) O on Cu_3/p-Mo_2CO_2.

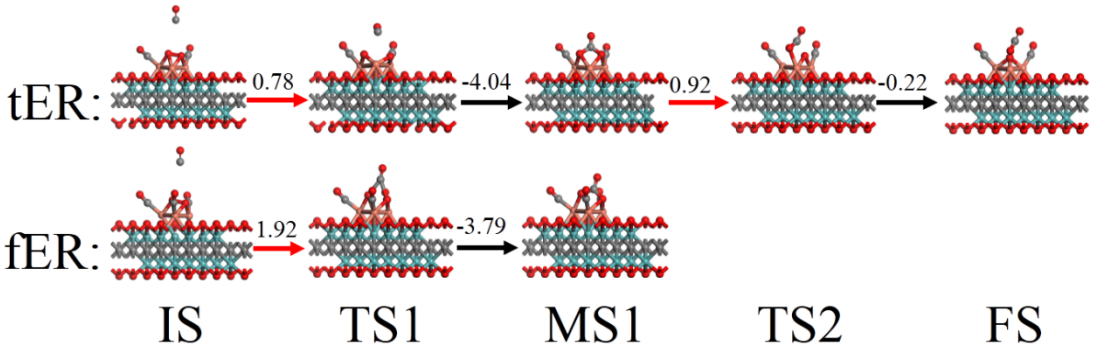

Figure S4. Reaction pathways (side views) of CO oxidation on Cu_3/d-Mo_2CO_2 via the tER (t: termolecular, three CO molecules), and fER (f: tetramolecular, four CO molecules) involved in the O_2-parallel configuration. IS, TS1, MS1, TS2 and FS denote the initial state, first transition state, first intermediate state, second transition state and final state, respectively. The numbers above the red and black arrows represent the activation barriers and reaction energies, respectively. The energy values are shown in unit of eV.

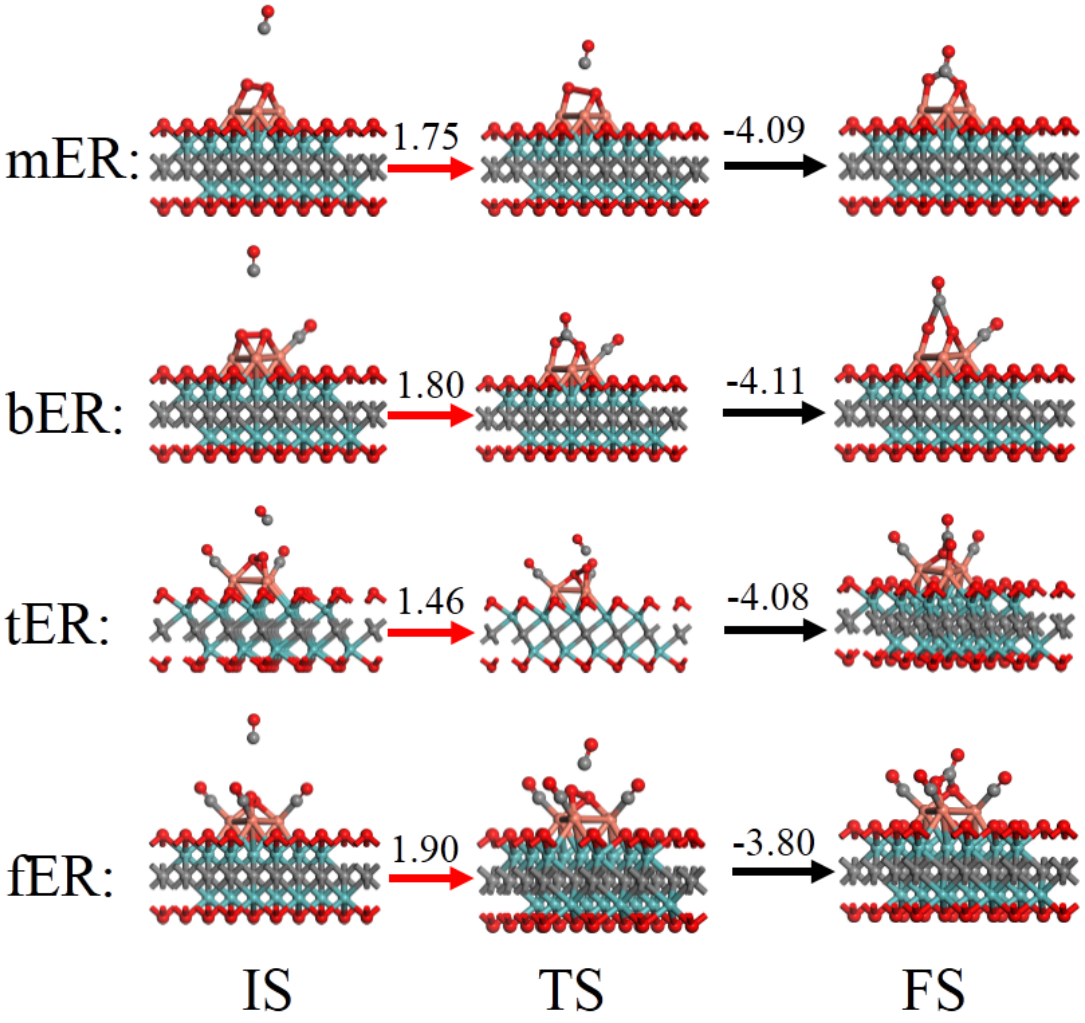

Figure S5. Reaction pathways (side views) of CO oxidation on Cu_3/d-Mo_2CO_2 via the mER (m: monomolecular, single CO molecule), bER (b: bimolecular, two CO molecules), tER (t: termolecular, three CO molecules), and fER (f: tetramolecular, four CO molecules) involved in the O_2-diagonal configuration. IS, TS1, MS1, TS2 and FS denote the initial state, first transition state, first intermediate state, second transition state and final state, respectively. The numbers above the red and black arrows represent the activation barrier and reaction energies, respectively. The energy values are shown in unit of eV.

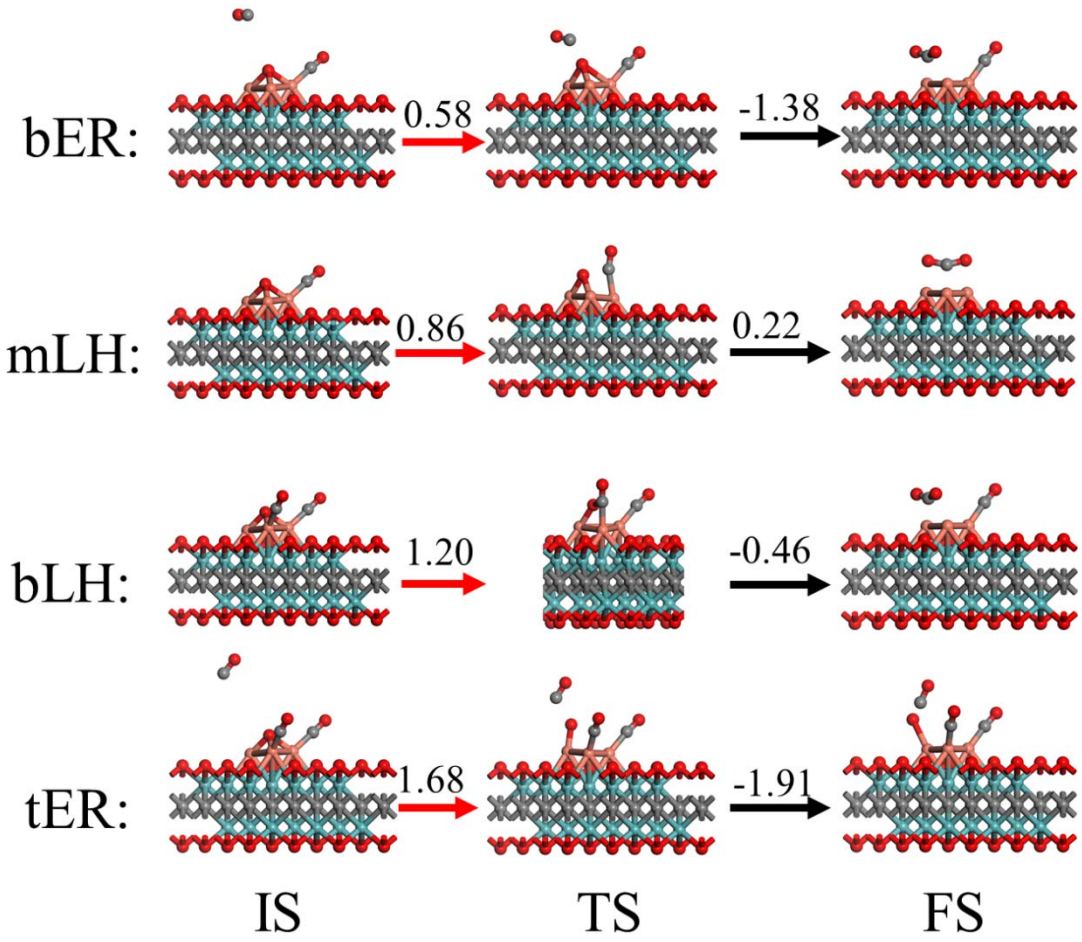

Figure S6. Reaction pathways (side views) of CO oxidation on Cu_3/d-Mo_2CO_2 via the bER (b: bimolecular, two CO molecules), mLH (m: monomolecular, single CO molecule), bLH (b: bimolecular, two CO molecules), and tER (t: termolecular, three CO molecules) involved in the O_2-diagonal configuration. IS, TS1, MS1, TS2, and FS denote the initial state, first transition state, first intermediate state, second transition state and final state, respectively. The numbers above the red and black arrows represent the activation barriers and reaction energies, respectively. The energy values are shown in unit of eV.

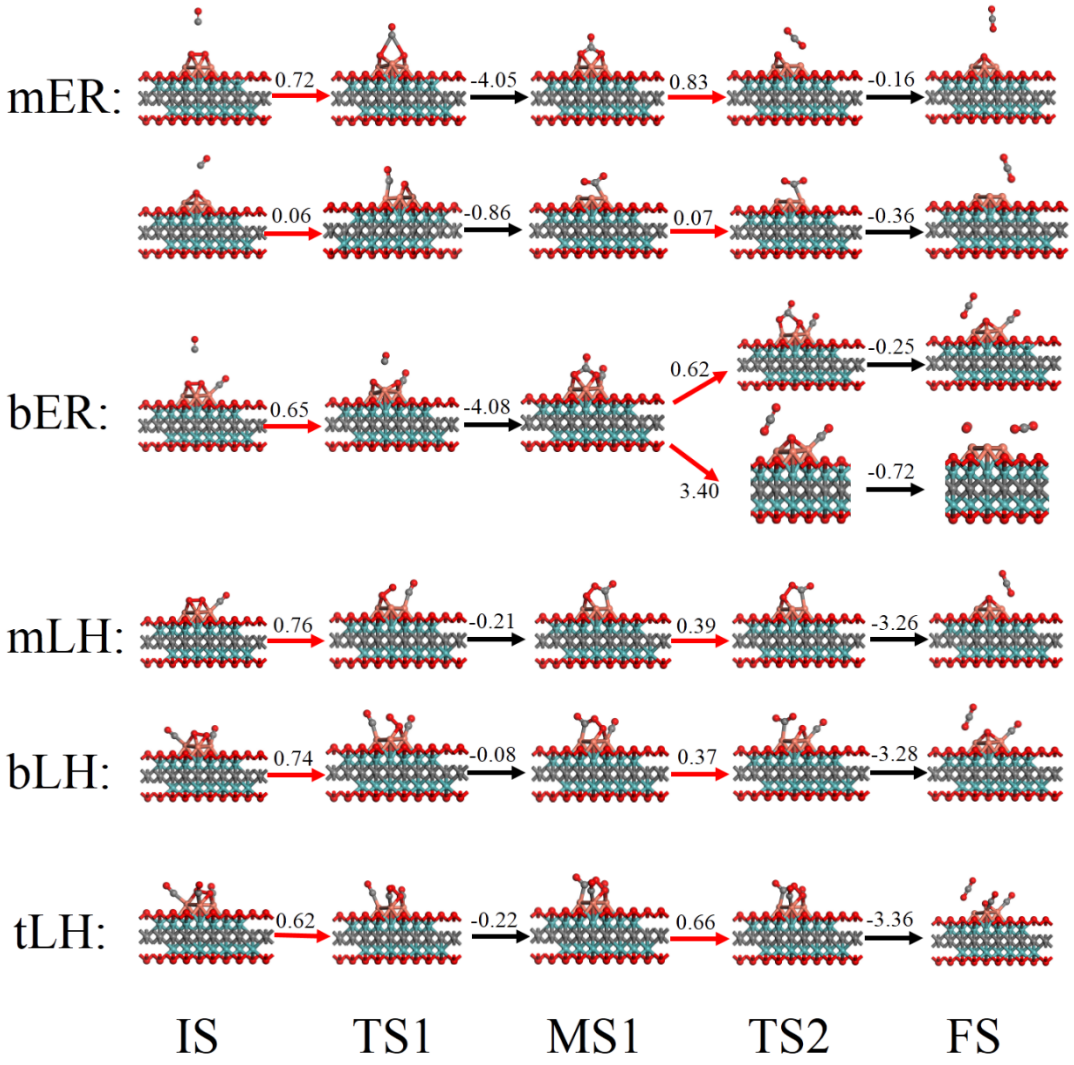

Figure S7. Reaction pathways (side views) of CO oxidation on Cu_3/d-Mo_2CO_2 via the mER, bER, mLH, bLH and tLH mechanism involved in the O_2-parallel configuration, where m, b and t represent monomolecular (only one CO molecule), bimolecular (two CO molecules), and termolecular (three CO molecules), respectively. IS, TS1, MS1, TS2 and FS denote the initial state, first transition state, first intermediate state, second transition state, and final state, respectively. The numbers above to the red and black arrows represent activation barriers and the reaction energies, respectively. The energy values are shown in unit of eV.

Part I. Details of analysis for why we choose Cu_3 cluster on the defective Mo_2CO_2 monolayer.

The three-atom transition metal clusters have been proved with high activity towards many chemical processes based on the first principles calculations, including CO oxidation. For instance, Zeng's group[1] found that the unique triangular Au_3 active site played a vital role in promoting the CO oxidation. Jiang's group[2] found that Cu_3 active site anchored on MoS_2 played an important role in catalyzing CO oxidation. Li's group[3] reported that Fe_3 anchored on Al_2O_3 as a single cluster catalyst exhibited unusual activity for ammonia synthesis. Especially, many excellent works from Sunney Chan's laboratory[4-5] demonstrated that Cu_3 active site of tricopper cluster complex within enzyme systems exhibited novel oxygen reduction reaction activity and methanol synthesized activity. Their studies also provided the synthesis methods on enzyme systems. It might be anticipated that these methods would be applicable to prepare Cu_3 on other substrates like Mo_2CO_2, which has many outstanding properties. We also expect that the outstanding properties of Cu_3 active site would be displayed on Mo_2CO_2. Therefore, we chose Cu_3 cluster on Mo_2CO_2 as a single-cluster catalyst to investigate the CO oxidation activity.

The characteristics of the defects at the surface will influence the formation of Cu clusters and their stability shown in Figure S8 and S9. Therefore, we calculated oxygen vacancy formation energies, and found that cluster with three vacancies is likely to form. Only neutral oxygen vacancies were considered with the formation energy defined as:

$$E_{\text{form}} = E_{\text{n}V} + nE_{1/2O_2} - E_P \quad (1)$$

where E_{nV}, $E_{1/2O_2}$, E_P, n are the total energies of the monolayer Mo_2CO_2 with oxygen vacancies, half of the O_2 molecule, primitive 2D Mo_2CO_2 and the number of oxygen vacancies, respectively. The formation energy of single oxygen vacancy of Mo_2CO_2 is 3.64 eV as given in our recent work[6]. Various oxygen vacancy configurations (n = 2, 3 and 4) are considered in the Figure S8, and the corresponding formation energies for the different configurations are shown in Table S1. Note that, the formation energies are similar when the number of vacancies are the same. However, when the number of oxygen vacancy is up to four, the quite large formation energies may inhibit its formation.

The Cu atoms anchored on the vacancies of the above-mentioned configurations are also shown in the Figure S9. The corresponding average binding energy, adhesion energy and cohesive energy

are calculated according to the equations in the "computational details", and the calculated results are summarized in the Table S2. According to the previous studies[7-8], metal atoms are inclined to aggregate into big clusters if the binding energy are weaker than the bulk cohesive energy. The binding energy of a single Cu atom on the surface with a single vacancy is about 0.16 eV lower than the Cu bulk cohesive energy. That's to say, Cu atoms have a tendency to aggregate into big cluster instead of keeping isolation. This fact agrees well with the calculated binding energies shown in Table S2 that the energetically favorable configurations are the closed forms (triangular configuration of Figure S9e, quadrangular configuration of Figure S9f and trapezoidal configuration of Figure S9i) with the biggest binding energies. Although the average binding energy per Cu in Figure S9e configuration is the same with the other two configurations displayed as Figure S9f and S9i, the adhesion energy ($E_{Cu-substrate}$), which represents as a measure of binding strength between the supported atoms and substrate, of Cu_3 shown in Figure S9e is larger than the other two, which guarantees Cu_3 shown in Figure S9e the most stable structure among all the structures ($n \leqq 5$). Therefore, Cu_3 cluster in a triangular configuration deposited on defective Mo_2CO_2 substrate would be the most energetically favorable configuration. Moreover, the oxygen vacancy formation energies of n = 4, 5 are larger than n = 3, we therefore choose triangular oxygen vacancies as the model, which is just compatible to the lowest energy Cu_3 cluster. Moreover, the existence of superficial vacancies of MXene has been confirmed by electron energy loss spectroscopy and atomic-resolution scanning transmission electron microscopy experiments[9-10]. In addition, the lowest energy structures of free Cu_n ($n \leqq 5$) clusters are 2D, and the triangular Cu_3 cluster may be prepared by soft-landing cluster method or thermal treatment analogous to the report of Li et al.[3].

After considering the formation energy and geometric stability of the supported Cu_3 cluster, we also consider its CO oxidation reactivity. For single Cu atom adsorbed on the defective substrate, the adsorption energies of CO, O_2 and CO_2 are -1.35, -0.53 and -0.59 eV, respectively. The weaker adsorption of O_2 than CO would give rise to the CO-poisoning problem. Meanwhile, the similar adsorption strength of O_2 and CO_2 will make them competitively dominating the active site. Therefore, we speculate the weak activity for CO oxidation on single Cu anchored Mo_2CO_2. When two Cu atoms are anchored on the defective Mo_2CO_2 with the configuration shown in Figure S9a, the long distance between the two Cu atoms make this system possessing the characteristics as the

single Cu anchored system that we do not consider this condition. We therefore consider the other configurations as shown in the Figure S9b. However, the desorption of CO_2 is difficult with reaction barriers of 0.83 eV (Figure S10), which is much bigger than that on Cu_3/d-Mo_2CO_2 (0.07 eV). Therefore, the one or two Cu atoms embedded systems possess poor activity and we do not consider them. Even though the sizes of the oxygen vacancies on Mo_2CO_2 surface are very large ($n \geqq 4$), after the deposition of three Cu atoms, the O_2 molecule can automatically dissociate with the dissociative oxygen atoms filling the vacancies, resulting in the sCu_3/d-Mo_2CO_2 configuration. Therefore, we focus on considering Cu_3/d-Mo_2CO_2 configuration.

To sum up, some three-atom transition metal clusters have been proved with high activity towards many chemical processes based on the first principles calculations, including CO oxidation[1-3]. Especially, many excellent works from Sunney Chan's laboratory[4-5] demonstrated that Cu_3 active site of tricopper cluster complex within enzyme systems exhibited novel oxygen reduction reaction activity and methanol synthesized activity. Their studies also provided the synthesis methods on enzyme systems. It might be anticipated that these methods would be applicable to prepare Cu_3 on other substrates like Mo_2CO_2, which has many outstanding properties. We expect that the outstanding properties of Cu_3 active site would be displayed on Mo_2CO_2. Therefore, we chose Cu_3 cluster on Mo_2CO_2 as a single-cluster catalyst to investigate the CO oxidation activity. Moreover, the existence of superficial vacancies of MXene has been confirmed by electron energy loss spectroscopy and atomic-resolution scanning transmission electron microscopy experiments[9-10]. The lowest energy structures of free Cu_3 cluster are 2D, and the triangular Cu_3 cluster may be prepared by soft-landing cluster method or thermal treatment analogous to the report of Li et al.[3] Even though the sizes of the oxygen vacancies on Mo_2CO_2 surface are very large ($n \geqq 4$), after the deposition of three Cu atoms, the O_2 molecule can automatically dissociate with the dissociative at the vacancies left with the dissociative oxygen atoms filling the vacancies, resulting in the Cu_3/d-Mo_2CO_2 configuration. Besides, the oxygen vacancy formation energies of n = 4, 5 are larger than that of n = 3, we therefore choose triangular oxygen vacancies as the model, which is just compatible to the Cu_3 cluster. Therefore, we focus on considering the Cu_3/d-Mo_2CO_2 configuration.

Here, we expect triangular Cu_3 cluster on the defective Mo_2CO_2 substrate namely Cu_3/d-Mo_2CO_2 as shown in Figure 1b or S9e is the best catalyst according to the formation energy,

geometric stability and reaction activity. We therefore only consider the Cu_3 instead of Cu_2 or Cu_4 or others. Additionally, the comparison with reference 33 is considered for the point that although there is no precise report about Cu cluster on Mo_2CO_2 so far, many metal nanoparticles (such as Pt, Au, Ag and so on) have been successfully synthesized on the MXene according to the hydrothermal synthesis, sputtering, atomic layer deposition (ALD) methods and one-step soft solution processing[11-14]. We hope the synthesis method in reference 33 is also applicable for the synthesis of Cu_3 cluster on Mo_2CO_2 since the flexibility and multiformity of synthesized composites on MXenes. The synthetic methods are the main goals here instead of the reaction processes. The chemical processes might be investigated in the next work.

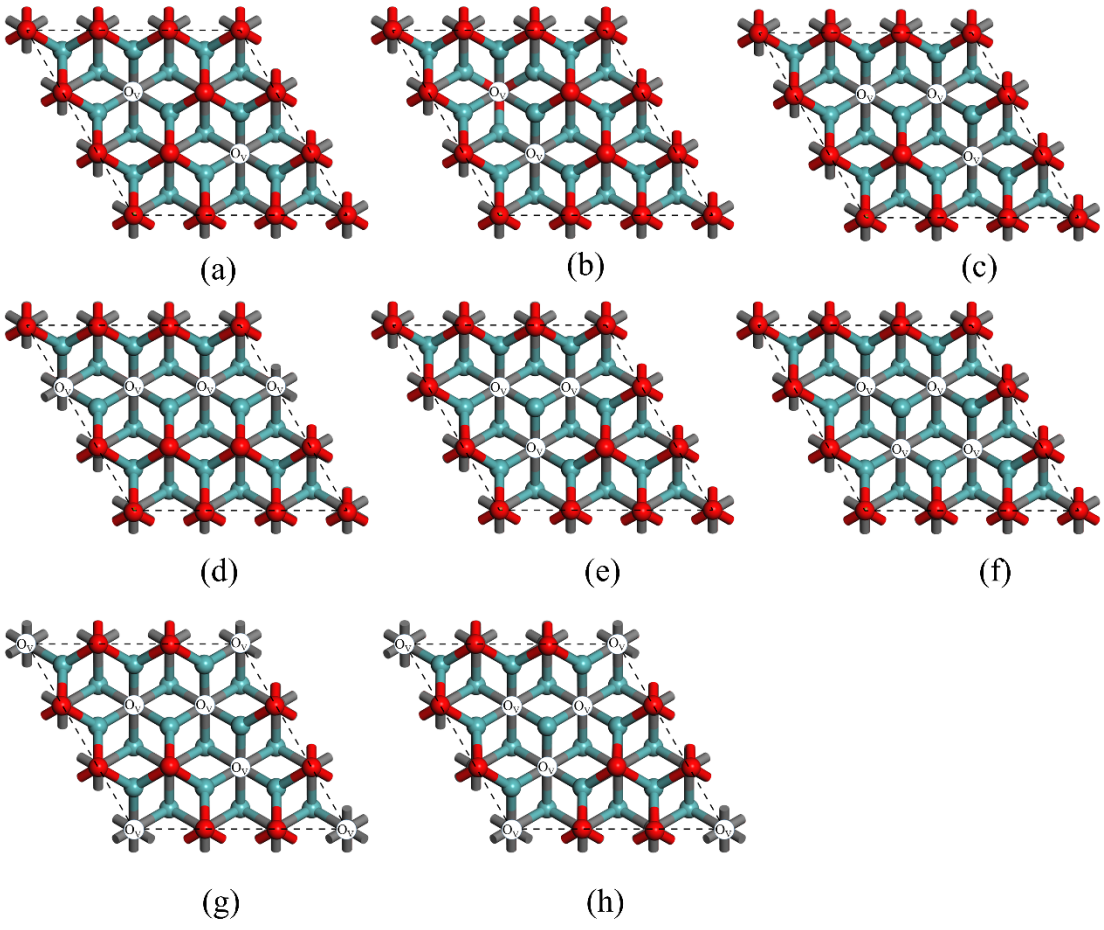

Figure S8. Top views of the different oxygen vacancy configurations ((a-b): n = 2; (c-e): n=3 and (f-h): n=4). The white areas represent oxygen vacancies.

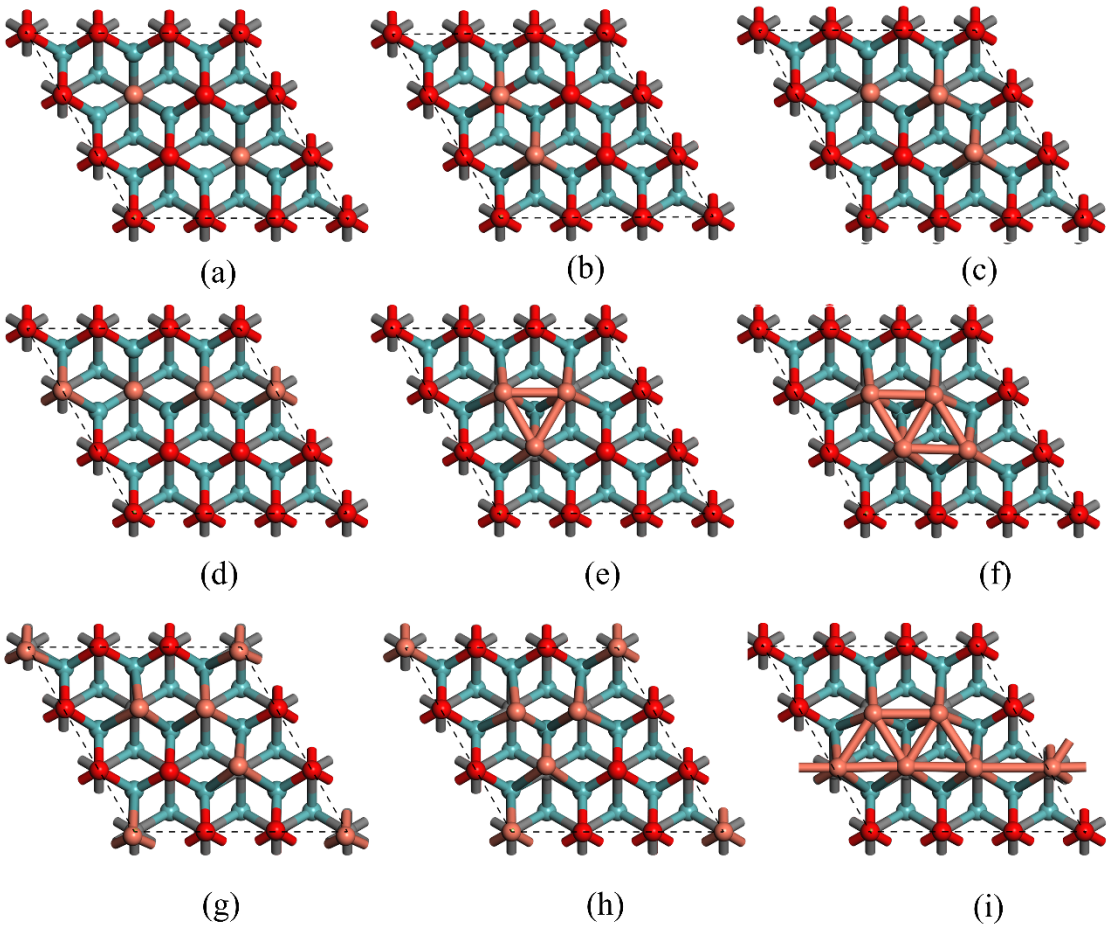

Figure S9. (a~h) Top views of the different adsorption configurations of Cu atoms anchor on various vacancies. (i) The lowest adsorption configuration for Cu_5 on the substrate.

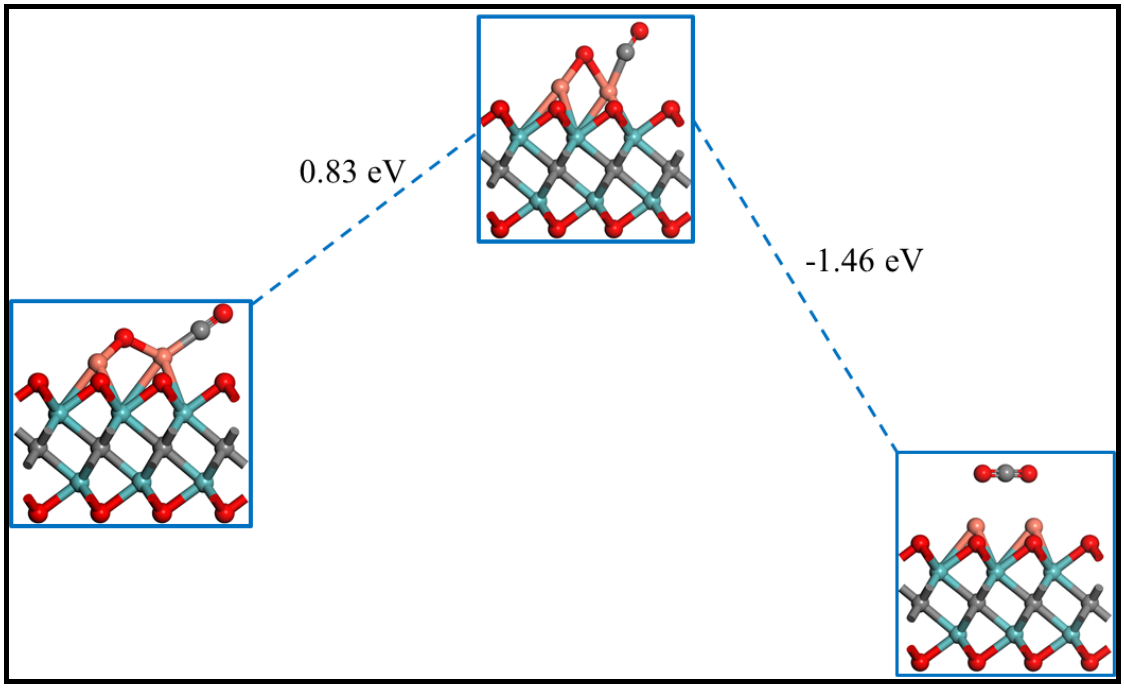

Figure S10. The reaction processes of the formation of CO_2 on two near Cu atoms embedded Mo_2CO_2 system (Figure S9b).

Table S1. The formation energies $E_{form}(nO_V)$ for various oxygen vacancy configurations (n = 2, 3 and 4) shown in Figure S8.

Configurations	$E_{form}(nO_V)$ (eV)
Figure a	7.44
Figure b	7.39
Figure c	11.31
Figure d	11.36
Figure e	11.40
Figure f	15.40
Figure g	15.32
Figure h	15.45

Table S2. The calculated average binding energy (E_b), adhesion energy ($E_{Cu-substrate}$), and cohesive energy (E_{Cu-Cu}) for the supported Cu atoms on vacancies configurations shown in Figure S9. The energies are shown in the unit of eV.

Configurations	E_b (eV)	$E_{Cu-substrate}$	E_{Cu-Cu}
Figure a	-3.66	-3.61	-0.05
Figure b	-3.63	-2.83	-0.80
Figure c	-3.56	-2.56	-1.00
Figure d	-3.50	-2.34	-1.16
Figure e	-3.75	-2.56	-1.19
Figure f	-3.75	-2.26	-1.49
Figure g	-3.48	-2.44	-1.04
Figure h	-3.66	-2.22	-1.44
Figure i	-3.76	-2.06	-1.70

Part II. More detailed derivations about the reliable activation barrier to depict the activity.

Generally, the computed reaction barriers (ΔEs) was used to compute the forward and backward reaction rates. For surface reactions, the reaction rates (k) for elementary reaction steps were determined by the Eyring equation[15]:

$$k = A\mathrm{e}^{\frac{-\Delta E}{K_b T}} \quad (2)$$

where ΔE, K_b, T and A are the reaction barrier, Boltzmann constant, temperature and prefactor, respectively. For convenience, the pre-factor A is always set to a constant for all the elementary surface reactions[16-17]. Obviously, the reaction rate k is exponentially related to reaction barrier. The critical reaction barrier for CO oxidation reaction is about 1.0 eV at room temperature according to previous reports[17-18]. In fact, for convenience, researches are always choosing reaction barrier (ΔE) as the effective judgment for results[19-21].

Part III. Detailed calculated methods for non-neutral defects on Mo_2CO_2 monolayer.

It is relatively complicated to obtain the formation energies of non-neutral defects. The calculated methods are listed below as that given by Zhang and Northrup[22]. The formation energy ($\Delta H_{form}(O^Q)$) of a defect O in the charge state Q is defined as

$$\Delta H_{form}(O^Q) = E_{tot}(O^Q) - \sum_X n_X \mu_X + Q(\mu e + E_v) + M(Q) \quad (3)$$

where μ_e is the electron chemical potential (equaling the Fermi level E_f in the T = 0 K calculations), $E_{tot}(O^Q)$ is the total energy of the defective supercell in the charge state Q, E_v is the top valence band energy, M(Q) is the defect-dependent multipole corrective term of reference[23] [Phys. Rev. B 1995, 51 (7), 4014-4022], n_X and μ_X are the number of involved atoms (X = Mo, C, O) and their chemical potentials, respectively. The chemical potential of involved atoms are not independent variables, since their species are in equilibrium with the Mo_2CO_2 bulk compound. Their chemical potentials must satisfy the following condition:

$$\mu^{bulk}_{Mo_2CO_2} = 2\mu_{Mo} + \mu_C + 2\mu_O \quad (4)$$

Part IV. The influence of the adsorbed reactants on the support at the vicinity of the Cu_3 cluster.

As shown in Figure 4, O_2 has a stronger binding strength than CO and therefore will first dominates the active site when they are occurring simultaneously. However, the second O_2 has a weak adsorption at the active site and CO will overwhelm the second O_2 and dominates the active site as displayed in Table 2. The weak adsorption of the second O_2 is found from the fact that when we put an O_2 slightly away from the active site, it will be physically adsorbed on the surface as displayed in Figure S11. The Cu_3 cluster keeps neutral when the first O_2 dominates the active site and the second O_2 appears in the vicinity of the active site simultaneously. The second O_2 has a weak adsorption at the active site and CO molecules will overwhelmingly dominate the active site as displayed in Table 2.

However, no matter where the CO molecules initially are, they intend to diffuse to the Cu_3 active site as shown in Figure S12 of the different adsorption sites. In other word, CO would not be adsorbed at the vicinity of the Cu_3 cluster and will rapidly take part in the reaction. So, the adsorption of the reactants on the support would not influence the charge transfer between the support and the cluster, and not influence the reaction path and the oxidation ability of the cluster.

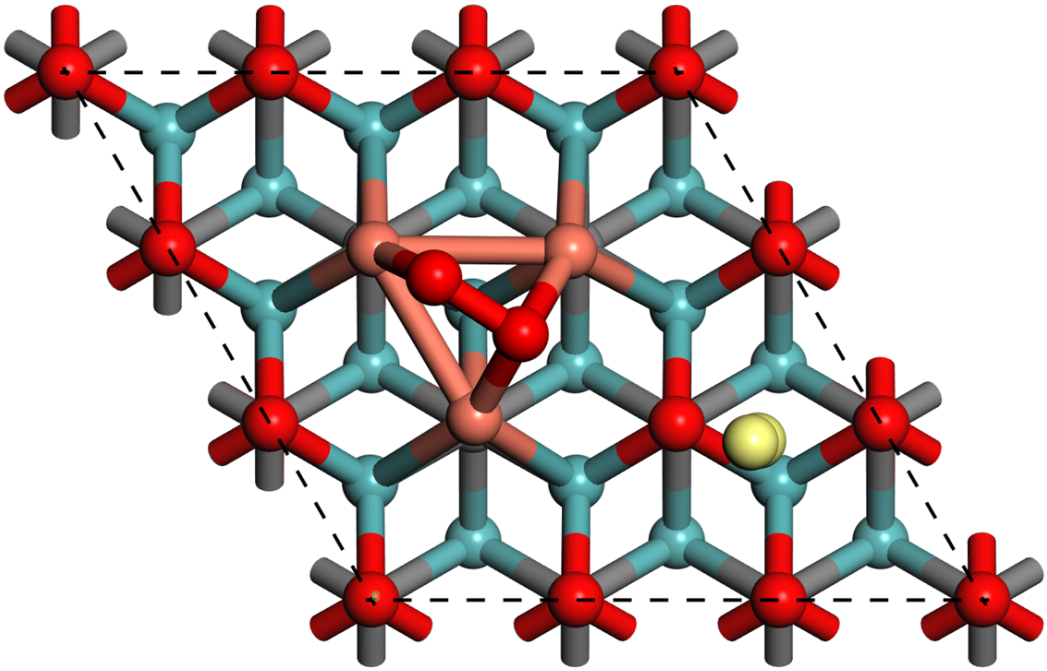

Figure S11. The geometric structure of the first O_2 dominates the active site and the second O_2 physically adsorbs in the vicinity of the surface. The red, blue, grey, and orange balls represent

the O, Mo, C, and Cu atoms, respectively. The yellow balls represent the second adsorbed O_2.

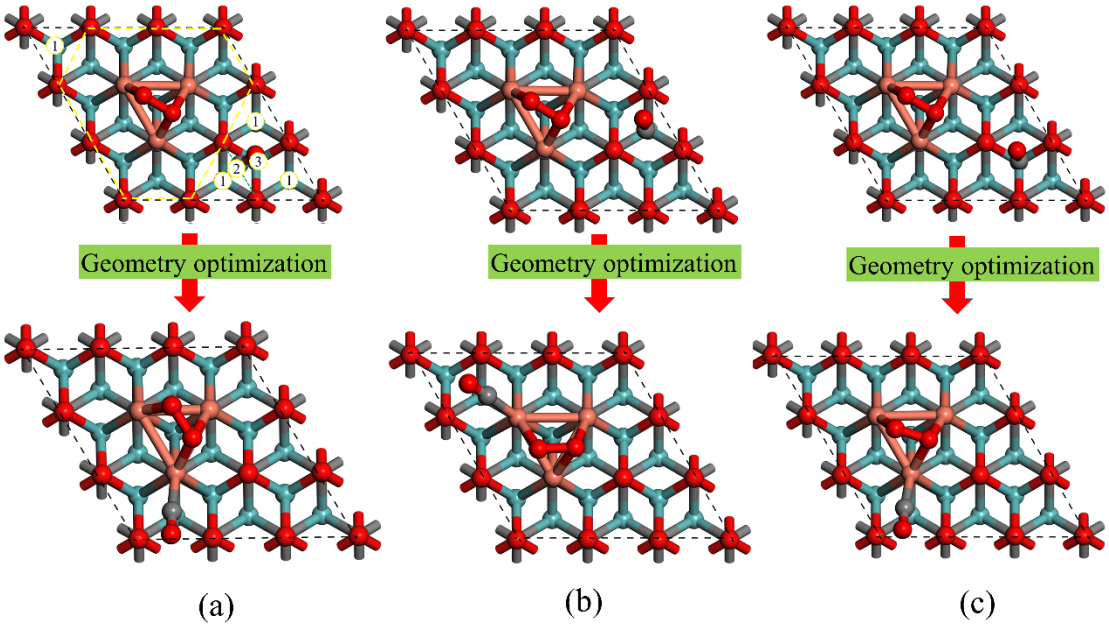

Figure S12. The structures of the coadsorbed structures of (CO + O_2) before and after optimizing geometric structures. One O_2 is first diagonally adsorbed on the Cu_3 active site, and one CO molecule is physically adsorbed at the vicinity of the different active sites, which are labeled as 1, 2 and 3. (a-c) Structures shown in the upper panels with CO molecule adsorbs at sites 3, 1, and 2 before geometry optimization, and the corresponding structures after geometry optimization shown in the bottom panels.

Part V. The reaction mechanisms involved in the O_2-parallel configuration.

ER Mechanism. Because the adsorption energies of O_2 is lower than CO, we guess that O_2 can dominantly take up the active sites when mixed gases of CO and O_2 are injected into the catalyst. Therefore, the CO oxidation reaction would follow the ER mechanism (Figure S7, mER), where the first physically adsorbed CO gradually approaches the pre-adsorbed O_2 and then forms the CO_3 intermediate with a barrier of 0.72 eV. The dissociation of the CO_3 intermediate to release the first CO_2 is slightly harder with the activation barrier of 0.83 eV. To proceed, the remained atomic O can be easily removed by oxidizing with the forthcoming CO and releasing the second CO_2 with the maximum barrier of 0.07 eV as shown in Figure S7. Besides, more than one CO molecules can be adsorbed according to the above calculation. The physically adsorbed CO approaching the substrate with the co-adsorbed oxygen and one CO is assumed as bER mechanism. The detailed reaction pathways can be seen in bER of Figure S7. There appears a CO promotion effect to form CO_3 intermediate with a smaller activation barrier of 0.65 eV, and then desorb first CO_2 molecule with the reaction heat of 4.33 eV releasing in the whole process. In contrast, the formation of two CO_2 at the same time is difficult with a huge barrier of 3.40 eV. Also, when CO molecules at high concentration, the cases that a physically adsorbed CO increasingly closes to the surface with two (tER in Figure S4) or three (fER in Figure S4) CO molecules co-adsorbed with O_2 at parallel configuration on the substrate are considered as shown in Figure S4. The above two cases may be hard to happen as compared with the mER and bER mechanisms shown in Figure S7, because of the high rate-determining energy barriers (0.92 and 1.92 eV) for forming the first CO_2 (MS1 → FS, in Figure S4) and the CO_3 intermediate (IS → MS1, in Figure S4), respectively.

LH Mechanism. The LH mechanisms of one, two, or three CO molecules co-adsorbed with O_2 at parallel configuration on the substrate are shown at Figure S7 as mLH, bLH and tLH, respectively. For the mLH mechanism, one adsorbed CO can react smoothly with the co-adsorbed O_2 to construct the intermediate MS1 (in mLH) and release the first CO_2 (MS1 → FS, in Figure S7) with the barriers of 0.76 and 0.39 eV, respectively. As for the bLH mechanism, it has the similar effect to the mLH mechanism, indicating that the co-adsorption of more than one CO molecules cannot obviously promotes the reaction with the rate-limiting step barriers (0.74 eV) for forming the OOCO*

intermediate state (MS1 in bLH of Figure S7). After releasing a CO_2, atomic O and a co-adsorbed CO are left on the Cu_3 active site. But the release of the second CO_2 is easier via bER than mLH mechanism through comparing the energy barriers (0.58 vs 0.86 eV) as shown in Figure S6. In addition, since the same structure for MS1 in bLH in Figure S7 and Figure 5, the release of two CO_2 is considered shown in Figure 5 (MS1 → FS) with the barrier of 0.38 eV. In other word, in the bLH mechanism, the release of two CO_2 at the same time is preferred while the rate-limiting step is still the formation of OOCO* intermediate (MS1 in bLH of Figure S7). For the case of three CO co-adsorbed with the O_2 at parallel configuration on the substrate, the reaction called tLH mechanism in Figure S7 is smoother with a smaller barrier (0.62 eV). But the release of the first CO_2 has a slightly higher barrier than those of the mLH and bLH mechanisms (0.66 eV vs 0.39 and 0.37 eV). Once the first CO_2 is released, there leave an atomic O and two CO co-adsorbed on the substrate. However, the release of the second CO_2 is greatly harder with the barriers of 1.20 and 1.68 eV in the bLH and tER mechanisms shown in Figure S6. We also take into account the release of two CO_2 at the same time. Due to the same configuration of MS1 in the tLH mechanism (Figure S7 and 5), the whole process is shown in the tLH (MS1 → FS) in Figure S7 with the barrier of 0.57 eV.

In conclusion, more CO molecules co-adsorbed with the O_2 at parallel configuration could not always accelerate the reaction. The bER mechanism is more favorable than the other ER mechanisms according to the energy barriers, because it may proceed a big cycle to release CO_2 (bER (Figure S7) → bER (Figure S6) → bLH (Figure S7, release two CO_2 at the same time) or tLH (Figure S7, release two CO_2 at the same time) → bLH (Figure S7, release two CO_2 at the same time). When the O_2 pre-adsorbs at parallel configuration, no matter how the reaction proceeds, the rate-limiting step of the whole reaction process is still the formation of OCOO* intermediate (MS1 in bLH of Figure S7). It may proceed with bLH mechanism directly, or carry out the tLH mechanism first to form two CO_2 simultaneously and then continually proceed with bLH mechanism with the same rate-limiting energy barrier of 0.74 eV.

Table S3. Rate constant k (s^{-1}) for the elementary reactions on Cu_3/d-Mo_2CO_2 via the bLH mechanism involved in the O_2-diagonal configuration for the formation of two CO_2 (FS) simultaneously.

T (K)	IS-MS1 (2CO + O2 → OCOO + CO)	MS1-FS (OCOO + CO → $2CO_2$)
200	7.6114×10^{-6}	2.7380×10^{3}
298.15	7.0150×10^{0}	3.8497×10^{6}
400	8.7244×10^{3}	1.6547×10^{8}
500	5.6570×10^{5}	1.4962×10^{9}

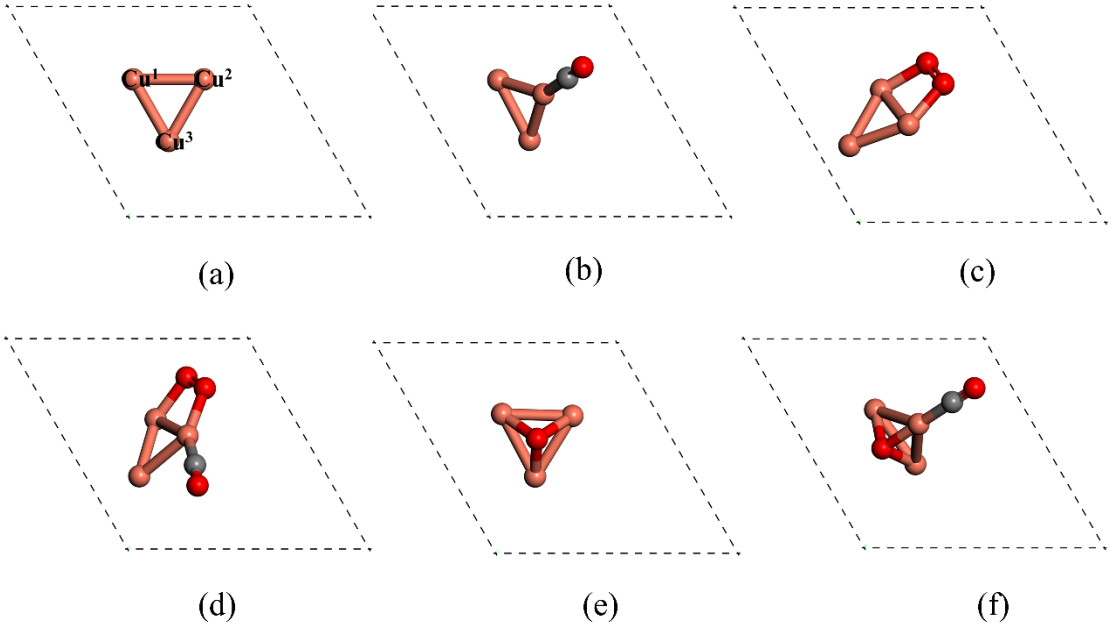

Figure S13 (a) Optimized triangular isolated Cu_3 cluster. (b-f) The geometric structures of CO oxidation intermediates adsorbed on Cu_3 cluster.

References:

1. Liu, C.; Tan, Y.; Lin, S.; Li, H.; Wu, X.; Li, L.; Pei, Y.;Zeng, X. C. CO Self-Promoting Oxidation on Nanosized Gold Clusters: Triangular Au_3 Active Site and CO Induced O–O Scission. *J. Am. Chem. Soc.* **2013,** *135* (7), 2583-2595.

2. Chen, Z. W.; Yan, J. M.; Zheng, W. T.;Jiang, Q. Cu_4 Cluster Doped Monolayer MoS_2 for CO Oxidation. *Sci Rep* **2015,** *5*, 11230.

3. Liu, J. C.; Ma, X. L.; Li, Y.; Wang, Y. G.; Xiao, H.;Li, J. Heterogeneous Fe_3 Single-Cluster Catalyst for Ammonia Synthesis Via an Associative Mechanism. *Nat Commun* **2018,** *9* (1), 1610.

4. Thiyagarajan, N.; Janmanchi, D.; Tsai, Y. F.; Wanna, W. H.; Ramu, R.; Chan, S. I.; Zen, J. M.;Yu, S. S. F. A Carbon Electrode Functionalized by a Tricopper Cluster Complex: Overcoming Overpotential and Production of Hydrogen Peroxide in the Oxygen Reduction Reaction. *Angewandte Chemie* **2018,** *130* (14), 3674-3678.

5. Liu, C.-C.; Mou, C.-Y.; Yu, S. S. F.;Chan, S. I. Heterogeneous Formulation of the Tricopper Complex for Efficient Catalytic Conversion of Methane into Methanol at Ambient Temperature and Pressure. *Energy Environ. Sci.* **2016,** *9* (4), 1361-1374.

6. Cheng, C.; Zhang, X.; Wang, M.; Wang, S.;Yang, Z. Single Pd Atomic Catalyst on Mo_2CO_2 Monolayer (MXene): Unusual Activity for CO Oxidation by Trimolecular Eley-Rideal Mechanism. *Phys. Chem. Chem. Phys.* **2018,** *20* (5), 3504-3513.

7. Deng, Q.; Zhao, L.; Gao, X.; Zhang, M.; Luo, Y.;Zhao, Y. Single Layer of Polymeric Cobalt Phthalocyanine: Promising Low-Cost and High-Activity Nanocatalysts for CO Oxidation. *Small* **2013,** *9* (20), 3506-3513.

8. Ma, D. W.; Wang, Q.; Yan, X.; Zhang, X.; He, C.; Zhou, D.; Tang, Y.; Lu, Z.;Yang, Z. 3 D Transition Metal Embedded C_2N Monolayers as Promising Single-Atom Catalysts: A First-Principles Study. *Carbon* **2016,** *105*, 463-473.

9. Sang, X.; Xie, Y.; Lin, M.-W.; Alhabeb, M.; Van Aken, K. L.; Gogotsi, Y.; Kent, P. R. C.; Xiao, K.;Unocic, R. R. Atomic Defects in Monolayer Titanium Carbide ($Ti_3C_2T_x$) MXene. *ACS Nano* **2016,** *10* (10), 9193-9200.

10. Karlsson, L. H.; Birch, J.; Halim, J.; Barsoum, M. W.;Persson, P. O. Atomically Resolved Structural and Chemical Investigation of Single MXene Sheets. *Nano Lett* **2015,** *15* (8), 4955-4960.

11. Ahmed, B.; Anjum, D. H.; Gogotsi, Y.;Alshareef, H. N. Atomic Layer Deposition of SnO_2 on MXene for Li-Ion Battery Anodes. *Nano Energy* **2017,** *34*, 249-256.

12. Satheeshkumar, E.; Makaryan, T.; Melikyan, A.; Minassian, H.; Gogotsi, Y.;Yoshimura, M. One-Step Solution Processing of Ag, Au and Pd@MXene Hybrids for Sers. *Sci Rep* **2016,** *6*, 32049.

13. Xie, X.; Chen, S.; Ding, W.; Nie, Y.;Wei, Z. An Extraordinarily Stable Catalyst: Pt Nps Supported on Two-Dimensional $Ti_3C_2X_2$ (X = Oh, F) Nanosheets for Oxygen Reduction Reaction. *Chem Commun (Camb)* **2013,** *49* (86), 10112-10114.

14. Zhang, Z.; Li, H.; Zou, G.; Fernandez, C.; Liu, B.; Zhang, Q.; Hu, J.;Peng, Q. Self-Reduction Synthesis of New MXene/Ag Composites with Unexpected Electrocatalytic Activity. *ACS Sustainable Chem. Eng.* **2016,** *4* (12), 6763-6771.

15. Eyring, H. The Activated Complex in Chemical Reactions. *J. Chem. Phys.* **1935,** *3* (2), 107-115.

16. Liu, J. X.; Su, Y.; Filot, I. A. W.;Hensen, E. J. M. A Linear Scaling Relation for CO Oxidation on CeO_2-Supported Pd. *J. Am. Chem. Soc.* **2018,** *140* (13), 4580-4587.

17. Jiang, Q. G.; Ao, Z. M.; Li, S.;Wen, Z. Density Functional Theory Calculations on the CO

Catalytic Oxidation on Al-Embedded Graphene. *RSC Adv.* **2014,** *4* (39), 20290-20296.
18. Alavi, A.; Hu, P.; Deutsch, T.; Silvestrelli, P. L.;Hutter, J. CO Oxidation on Pt(111): An Ab Initio Density Functional Theory Study. *Phys. Rev. Lett.* **1998,** *80* (16), 3650-3653.
19. Gong, X.-Q.; Liu, Z.-P.; Raval, R.;Hu, P. A Systematic Study of CO Oxidation on Metals and Metal Oxides: Density Functional Theory Calculations. *J. Am. Chem. Soc.* **2004,** *126* (1), 8-9.
20. Liu, Z.-P.; Gong, X.-Q.; Kohanoff, J.; Sanchez, C.;Hu, P. Catalytic Role of Metal Oxides in Gold-Based Catalysts: A First Principles Study of CO Oxidation on TiO_2 Supported Au. *Phys. Rev. Lett.* **2003,** *91* (26), 266102.
21. Qiao, B.; Wang, A.; Yang, X.; Allard, L. F.; Jiang, Z.; Cui, Y.; Liu, J.; Li, J.;Zhang, T. Single-Atom Catalysis of CO Oxidation Using Pt_1/FeOx. *Nat Chem* **2011,** *3* (8), 634-641.
22. Zhang, S. B.;Northrup, J. E. Chemical Potential Dependence of Defect Formation Energies in Gaas: Application to Ga Self-Diffusion. *Phys. Rev. Lett.* **1991,** *67* (17), 2339-2342.
23. Makov, G.;Payne, M. C. Periodic Boundary Conditions in Ab Initio Calculations. *Phys. Rev. B* **1995,** *51* (7), 4014-4022.